BAU Journal - Science and Technology

Volume 1 | Issue 1
ISSN: 2706-784X

Article 10

December 2019

MECHANICAL PROPERTIES OF TRANSITION METALS MN,FE AND ZN DOPED NIO NANOPARTICLES

Ahmed Khalaf
Faculty of Science, Damanhur University, Damanhur, Egypt, a_khalaf81@yahoo.com

Jamalat Al Boukhari
Faculty of Science, Beirut Arab University, Beirut, Lebanon, jamalat.boukhari@gmail.com

Lidea Zeidan
Faculty of Science, Beirut Arab University, Beirut, Lebanon, Lidea.zeidan@gmail.com

MECHANICAL PROPERTIES OF TRANSITION METALS MN,FE AND ZN DOPED NIO NANOPARTICLES

Abstract

This work is a continuation of the characterization study of nickel oxide (NiO) nanoparticles (NPs) doped with transition metals (TM) like Mn, Fe and Zn, synthesized by the co-precipitation method. In this part, the effect of TM doping on the physical and mechanical properties of the NiO NPs is examined using a digital Vickers microhardness tester. The microhardness measurement results enable us to evaluate the important mechanical parameters including Vickers microhardness (HV), Young's modulus (E), yield strength (Y) and fracture toughness (KIC), responsible for practical industrial applications. It was found that all the properties given above strongly depend on the type of TM doping element. Specifically, Vickers microhardness Hv values of the samples studied in this work were found to decrease by doping with Mn, Fe, and Zn. Moreover, the normal Indentation Size Effect (ISE) behavior was observed. The experimental results were analyzed according to Meyer's Law, Proportional Sample Resistance (PSR), Elastic/Plastic Deformation (EPD) models, and Hays–Kendall (HK) approach. As a result, the Hays–Kendall (HK) approach is found to be the best model for the load-independent microhardness determination of the studied samples.

Keywords

NiO nanoparticles - Co-precipitation - Transition metals - Mechanical properties.

1. INTRODUCTION

The interest in pure and doped NiO nanoparticles is increasing day by day because of their unique physical and electronic properties. Such properties have been found to be promising for the technological applications, such as electrochromic devices (He et al., 2018), smart windows (Yoshimura et al., 1995), optical fibers (Liu & Anderson, 1996), gas sensors (Hotovy et al., 2002), solar thermal absorbers (Cook et al., 1984), batteries (Makkus et al., 1994) and transparent conducting layers (Chan et al. 2002). Many researches reporting about the electrical, magnetic and optical properties of NiO NPs are available in the literature (Al Boukhari et al., 2019a, 2019b; Abdallah et al., 2019; Shahzad et al. 2015; Patel et al., 2018).

However, not enough studies can be found about the mechanical properties, which are related to the strength of these materials. The mechanical properties are mainly due to the interatomic forces. In addition, these properties may be greatly improved by internal structural modifications and extremely changed with various doping (Rajkovic et al., 2012; Farhat et al., 2019; Asikuzun et al., 2015; Kazah &Awad, 2017). The determination of the mechanical parameters such as hardness, Young's modulus, yield strength, and fracture toughness of NiO-based semiconductors is important for designing and fabricating the practical devices for applications such as electrical varistors, ultra-violet light emitters, transparent high-power electronics, and surface acoustic wave devices, window materials for display and spintronic devices (Tosun et al., 2014). For instance, Wang et al., (2019) studied the mechanical properties of Cu-doped NiO thin films at different annealing temperatures. The results revealed that that both the hardness and Young's modulus of the Cu-doped thin films increased with the annealing temperature. This is due to the prominent effect of grain boundaries and/or strain state in determining the mechanical properties. The doped Cu ions could be thermally assisted to occupy the Ni sites, and the ionic size difference, in turn, leads to the internal lattice strain.

In this work, microhardness values for pure NiO and TM (Mn, Fe, and Zn) doped NiO NPs are measured using Vickers microhardness tester for its common usage and nondestructive testing conditions regarding the sample surfaces. Different analytical models, such as Meyer's Law, Proportional Sample Resistance (PSR), Elastic/Plastic Deformation (EPD) models, and Hays–Kendall (HK) approach, were used to interpret the data obtained from Vickers microhardness test.

2. EXPERIMENTAL TECHNIQUES

In previous work (Al Boukhari et al., 2019b), pure NiO and 2 at% TM= Mn, Fe, and Zn doped NiO NPs were prepared via co-precipitation method at calcination temperature 550 °C. We reported the change of the microstructural, optical and magnetic properties of TM-doped NiO NPs samples by using transmission electron microscope TEM, proton induced X-ray emission PIXE, Rutherford back scattering RBS, Fourier transmission infrared spectroscopy FTIR, UV-vis spectroscopy, M-H loop as well as electron paramagnetic resonance EPR. In the present work, the Vickers microhardness of the pure and TM-doped NiO samples were measured using IN-412A microhardness tester at room temperature. The load was applied for 60 s and changed in the range of 0.50–10 N. The indentations were made at different regions of the sample surfaces to make sure that the indentations do not overlap.

3. REULTS AND DISCUSSION

Figure 1 displays the X-ray diffraction XRD patterns of pure and TM (Mn, Fe and Zn)-doped NiO NPs. The peak positions appearing at 2θ=37.3°, 44.4°, 62.83°, 76.3° and 79.3° which are indexed as (111), (200), (220), (311) and (222) crystalline planes, respectively. All the reflections reveal that the face-centered cubic (fcc) structure of NiO NPs was formed, without any evidence of impurity or secondary phases.

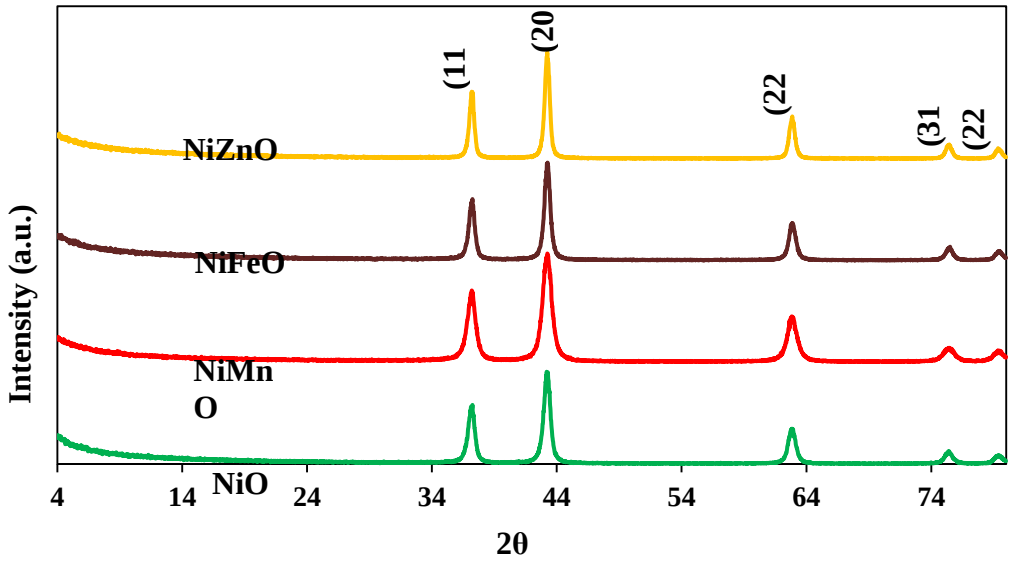

Fig. 1: XRD patterns of the pure and Tm (Mn, Fe and Zn) doped NiO nanoparticles.

The lattice parameter a, was calculated using Bragg's law:

$$a = d_{hkl}\sqrt{(h^2 + k^2 + l^2)}\,, \qquad (1)$$

where (hkl) are the Miller indices. The mean values of the lattice parameter a=4.185 ± 0.006 Å, listed in Table 1, are roughly the same for the all samples which may be due to the comparable values of the ionic radii (0.69 ± 0.05 Å).

The determination of crystallite size was based on Scherrer's formula (Cullity, B., 1967) using TOPAS software (BRUKER AXS):

$$D_{XRD} = \frac{K\lambda}{\beta cos\theta}, \qquad (2)$$

where λ is the X-ray wavelength, β is the full width at half maximum (FWHM), θ is the diffraction angle of the peaks and *K* is the Scherrer constant. Taking into consideration the instrument influence to the peak broadening βi, β was recalculated by the measured peak broadening according to the Eq. (Senthilkumar et al., 2009; Boukhachem et al., 2014):

$$\beta = \sqrt{\beta_m^2 - \beta_i^2} \qquad (3)$$

The average crystallite size as listed in Table 1, decreases upon doping NiO with the Mn^{2+} ions, and increases upon doping it with Fe^{3+} ions and Zn^{2+} ions. The variation in crystallite size could be attributed to the lattice disorder and strain induced by TM ions doping (Singh et al., 2009).

The dislocation densityδ, was calculated using the following formula (Bykkam et al., 2015):

$$\delta = \frac{1}{D_{XRD}^2}\,, \qquad (4)$$

The values of dislocation density (δ) are listed in Table 1. The highest density of dislocations, $\delta=4.255\times10^{15}$ line/m^2, is obtained for NiMnO. This may be due to the increased defects and voids in the NiO crystal structure that yields a smaller crystallite size (Gaber et al., 2014). This is consistent with that obtained from Scherrer's formula, where NiMnO NPs have the smallest crystallite size.

Table 1: The values of lattice parameter (a), crystallite size (D) and dislocation density (δ)

Samples	a [Å]	D [nm]	δx10^{15} [line/m^2]
NiO	4.189	22.77±1.94	1.929
NiMnO	4.185	15.33±1.50	4.255
NiFeO	4.179	25.40±2.51	1.550
NiZnO	4.184	33.33±2.32	0.900

3.1. Vickers Microhardness Measurements

It is known that, hardness is the resistance of a material against local plastic deformation. The Vickers microhardness values, H_v, of different applied loads in the range of 0.5–10 N for 60 s were calculated as:

$$H_v = 1854.4\frac{F}{d^2} GPa\,, \tag{5}$$

where F is the applied load in (N), and d is the mean diagonal length in (μm). Additionally, the values of the Young's modulus (E), yield strength (Y), fracture toughness (K_{IC}) and brittleness index (B_i) were calculated using Eqs (6-9) given below for all samples:

$$E = 81.9635 H_v\,, \tag{6}$$

$$Y \approx \frac{H_v}{3}\,, \tag{7}$$

$$K_{IC} = \sqrt{2E\alpha}\,, \tag{8}$$

$$B_i = H_v / K_{IC}\,, \tag{9}$$

where α is the surface energy. The variation of Vickers microhardness values against the applied load to the samples are displayed in Figure 2. It is clear that the microhardness values decline with the applied load for all the prepared samples. The behavior of nonlinearity is known as the Indentation Size Effect (ISE) (Gong et al., 1999). In other words, smaller indentation load shows a greater hardness value. When NiO NPs are doped with different TM (Mn, Fe and Zn) elements, the microhardness values decrease at the same applied load as compared to pure NiO NPs. The microhardness of Zn, Mn and Fe doped NiO NPs gradually decreased, respectively. This reduction is related to defects or irregularities, such as dislocation and grain boundaries (GBS) (Kumar et al., 2019). These factors weaken the strong ties and ultimately lead to reduced stiffness. Similar behavior for ZnMgO NPs doped with TM (Ni, Co, Mn, and Cr) was obtained by Arda et al., (2013).

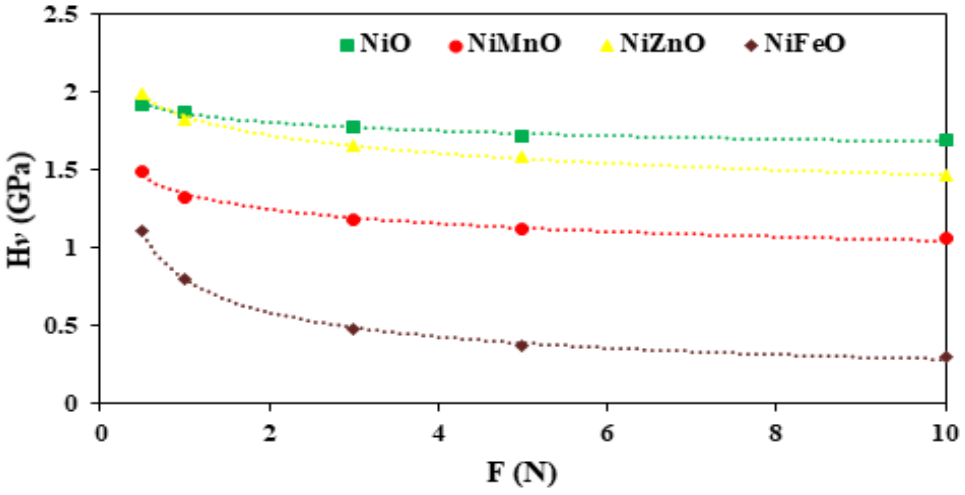

Fig.2: Variation of microhardness H_V versus load F for the samples.

As seen in Figure 2, the values of microhardness have reached a plateau (saturation region) at about 3 N for the samples of Zn and Mn doped NiO NPs and 5 N for Fe doped NiO NPs, respectively. Widely used models are presented in the next section in order to explain this ISE behavior.

3.2. Analyses and Modeling

3.2.1 Meyer's law

The general Meyer's law (Quinn et al., 1997), which relates the load F to the size d^{n_k}, is:

$$F = A_1 d^{n_k}\,, \tag{10}$$

where the exponent n_k is Meyer's number and A_1 is a constant. For normal ISE behavior, the exponent $n_k<2$ and for reverse ISE behavior the exponent $n_k>2$. When $n_k=2$, the hardness is independent of the applied load. The value of n_k is determined from the slope of ln(d) against ln(F) plot, as shown in Figure 3.

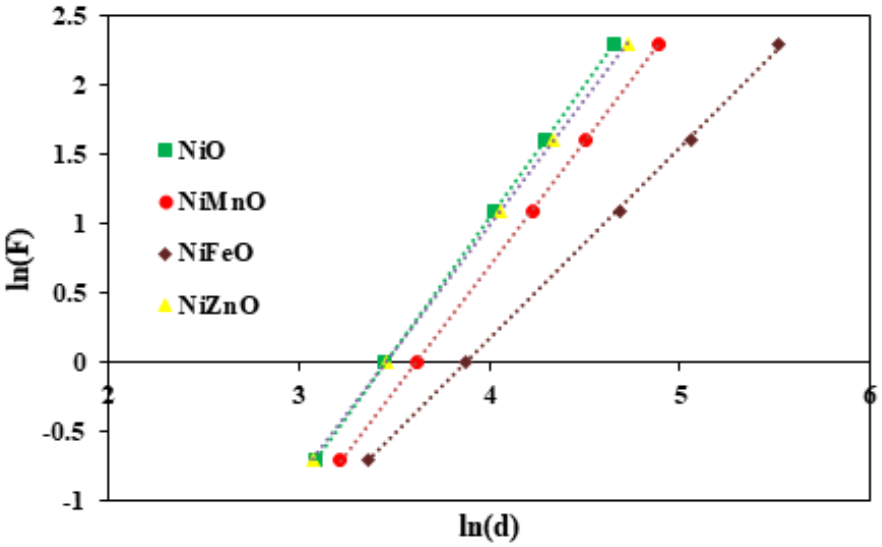

Fig.3: Variation of applied load ln(F) versus diagonal ln(d) for the samples.

The values of n_k are smaller than 2 for pure and Mn, Fe and Zn doped NiO NPs, confirming that the character of load-dependent displacement behavior is in the form of the reverse ISE behavior. The values of n_k and A_1 data are listed in Table 2.

Table 2: Best-fit results of experimental data according to Meyer's law

Samples	n_k	$A_1\times10^{-3}$ (GPa)	H_V (GPa)
NiO	1.91	1.35	1.716-1.690
NiMnO	1.80	1.49	1.125-1.060
NiFeO	1.38	4.73	0.376-0.300
NiZnO	1.82	1.86	1.582-1.460

3.2.2 Proportional Sample Resistance Model PSR

This model is used for the hardness analysis of materials having ISE behavior and given as follows (Li and Bradt., 1993):

$$\frac{F}{d}=\alpha+\beta d\,. \tag{11}$$

The values of α and β are estimated from (F/d)-d graph, as shown in Figure 4.

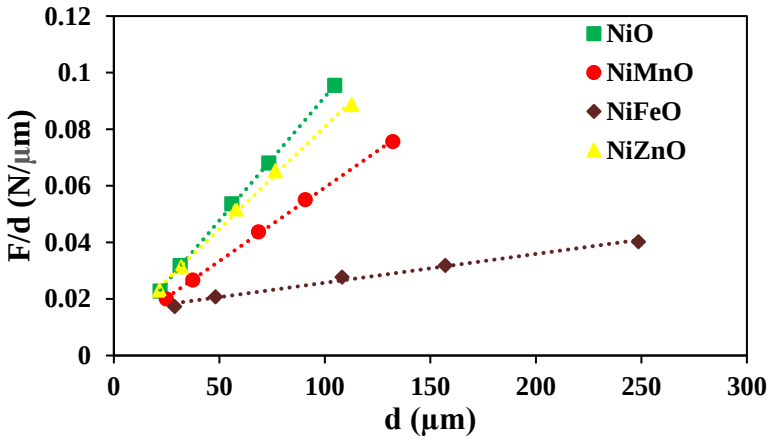

Fig.4: Plots of F/d versus d for the samples

It can be seen from Table 3, α is positive for all samples showing ISE behavior. The variation in α values is connected to the distribution of energy of the surface cracks [20]. β is a parameter that is used to obtain the real hardness value. In PSR model, load-independent hardness values are calculated according to:

$$H_{PSR} = 1854.4\beta . \quad (12)$$

Hardness values calculated in accordance with the PSR model (H_{PSR}), independent of the load, are given in Table 3. Transition values of the samples to the plateau region from Figure 2, are quite far from the hardness values independent of the load in PSR model. Hence, it is observed that the PSR model is not appropriate to determine the real hardness values of the materials.

Table 3: Best-fit results of experimental data according to PSR model

Samples	$\alpha\times10^{-2}$ (N/μm)	$\beta\times10^{-3}$ (N/μm^2)	H_{PSR} (GPa)	H_V (GPa)
NiO	0.40	0.90	1.67	1.716-1.690
NiMnO	0.74	0.50	0.93	1.125-1.060
NiFeO	1.56	0.10	0.19	0.376-0.300
NiZnO	0.86	0.70	1.30	1.582-1.460

3.2.3 Elastic/Plastic Deformation Model EPD

In this model, the dependence of the indentation size to the applied load is given below (Rahal et al., 2018):

$$F = A_2(d + d_o)^2 . \quad (13)$$

where A_2 is a constant and d_o is connected to the elastic deformation. A_2 and d_o values can be evaluated from $F^{1/2}$-d graph, as shown in Figure 5.

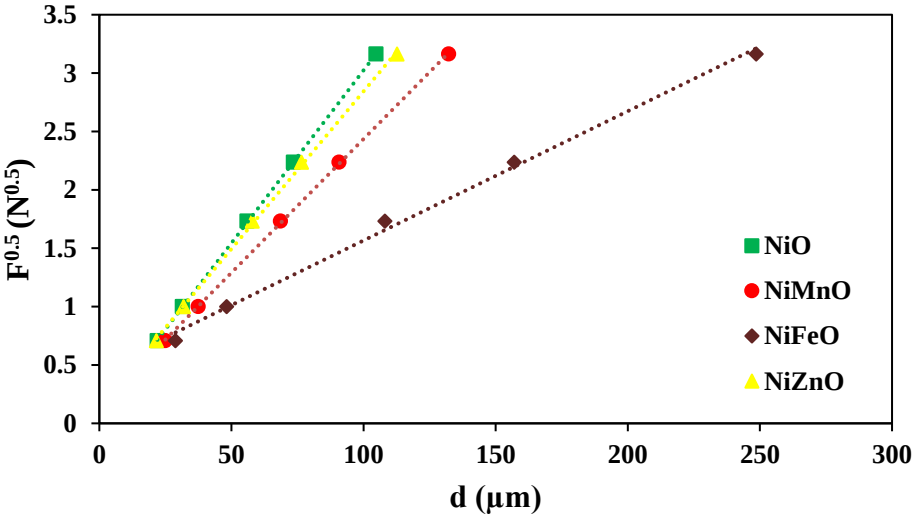

Fig. 5: Plots of $F^{0.5}$ versus d for the samples.

According to this model, d_o values are the points where the graph crosses the y-axis are positive since all the samples show the ISE behavior, as listed in Table 4. This is a proof that, for this range of applied loads, the elastic deformation is observed along with the plastic deformation. Thus, the elastic relaxation is present among the prepared samples (Srour et al., 2017). In this model, the load-independent hardness values are calculated as:

$$H_{EPD} = 1854.4A_2 , \quad (14)$$

Again, the hardness values calculated with this model are quite far from values in the plateau region. Therefore, the EPD model is not suitable for the hardness analysis of these materials.

Table 4: Best-fit results of experimental data according to EPD model.

Samples	$A_2 \times 10^{-3}$ (N/µm)	d_o (µm)	H_{EPD} (GPa)	H_V (GPa)
NiO	0.88	0.90	1.62	1.716-1.690
NiMnO	0.52	0.50	0.97	1.125-1.060
NiFeO	0.12	0.10	0.23	0.376-0.300
NiZnO	0.73	0.70	1.35	1.582-1.460

3.2.4 Hays-Kendall's Approach HK

According to this approach, load dependent hardness may be expressed by:

$$F = W_{HK} + A_{HK} d^2 \text{ ,(15)}$$

where W_{HK} is the minimum load to start plastic deformation and A_{HK} is the load-independent constant (Hayes and Kendall, 1973). The values of W_{HK} and A_{HK} can be estimated by plotting the experimental F against d^2 plot, as shown in Figure 6.

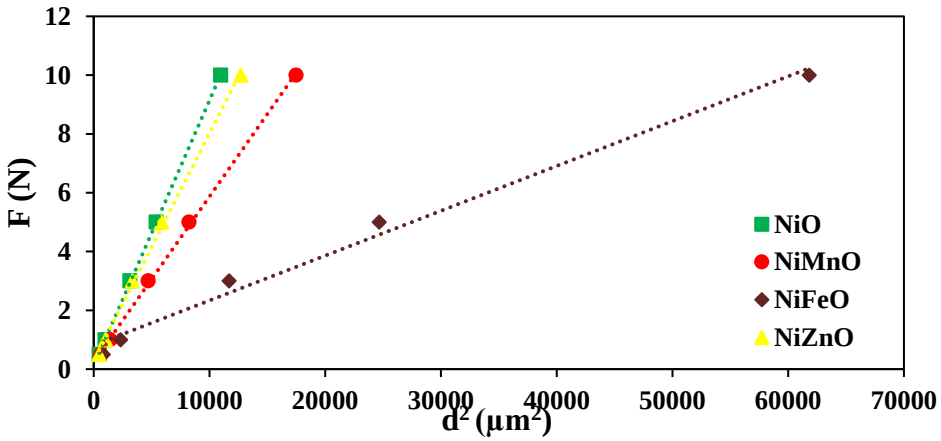

Fig. 6: Plots of F versus d^2 for the samples.

In this model, load-independent hardness values are as follows:

$$H_{HK} = 1854.4 A_{HK} \text{ .} \quad (16)$$

Load-independent hardness H_{HK}, W_{HK} and A_{HK} values are given in Table 5. Positive W_{HK} is the case observed in the samples, showing the ISE behavior. So, the applied load is interpreted to be sufficient for the elastic deformation. The hardness value obtained with HK approach is close to the hardness value in the plateau region. In studies of different materials in previous literature, it was emphasized that the hardness value, independent from the load, should be close to the hardness value of the plateau region (Gong et al., 2000; Peng et al., 2004). Therefore, HK approach is the most convenient model in the analysis of microhardness and in determining the mechanical properties of the samples showing the ISE behavior.

Table 5: Best-fit results of experimental data according to HK model.

Samples	$A_{HK} \times 10^{-5}$ (N/µm)	W_{HK} (N)	H_{HK} (GPa)	H_V (GPa)
NiO	90.30	0.110	1.68	1.716-1.690
NiMnO	56.20	0.253	1.11	1.125-1.060
NiFeO	15.30	0.810	0.37	0.376-0.300
NiZnO	74.70	0.278	1.48	1.582-1.460

Moreover, E, Y, K_{IC} and B_i values independent of the load are calculated with Eqs. (6-9) using-independent H_{HK} value. The obtained values are given in Table 4. It is seen from Table 6, E, Y and

K_{IC} values decrease for all samples. However, K_{IC} is important parameter for the selection of the materials in practical applications. Both elastic and plastic deformations are produced for the materials displaying the ISE behavior removed after the dipping. This situation leads to a quantity reduction of the material stiffness. The brittleness index is reduced since hardness reduced.

Table 6: The load independent, H_V, E, Y and K_{IC}

Samples	E (GPa)	Y (GPa)	K_{IC} (GPa/μm$^{1/2}$)	B_i (μm)	H_V (GPa)
NiO	137.25	0.558	1.05	1.598	1.716-1.690
NiMnO	91.20	0.371	1.16	0.958	1.125-1.060
NiFeO	30.40	0.124	0.98	0.381	0.376-0.300
NiZnO	121.60	0.495	1.45	1.026	1.582-1.460

4. CONCLUSIONS

$Ni_{0.98}TM_{0.02}O$ (TM=Mn, Fe, and Zn) were prepared as nanocrystalline powders via the co-precipitation method. It was observed that Vickers microhardness, modulus of elasticity, yield strength and fracture toughness values decreased with increasing applied load. The dependence of the load represented that normal ISE was observed for each sample. The experimental results of the microhardness measurements were analyzed using Meyer's law, PSR, EPD and HK approach. Based on the results obtained from the theoretical calculations, the HK approach was found to be the most suitable model that produces successful results exhibiting the ISE behavior of the samples.

REFERENCES

- Abdallah, M. A., Basma, H., Awad, R. (2019). Preparation, Characterization, and Application of Nickel Oxide Nanoparticles in Glucose and Lactose Biosensors. *Modern Applied Science*, 13, 6.
- Al Boukhari, J., Hassan, R. S., & Awad, R. (2019). Improving the Dielectric Behavior of Nio Nanoparticles by Samarium Doping For Electromagnetic Applications. *Materials Research Express*, *6*(11), 115094.
- Al Boukhari, J., Zeidan, L., Khalaf, A., Awad, R. (2019). Synthesis, Characterization, Optical and Magnetic Properties of Pure and Mn, Fe and Zn Doped Nio Nanoparticles. *Chemical Physics*, 516, 116-124.
- Arda, L., Ozturk, O., Asikuzun, E.,Ataoglu, S.(2013). Structural and Mechanical Properties of Transition Metals Doped Znmgo Nanoparticles. *Powder Technology*, 235,479484.
- Asikuzun, E., Ozturk, O., Arda, L., Akcan, D., Senol, S. D., Terzioglu, C. (2015). Preparation, structural and micromechanical properties of (Al/Mg) co-doped ZnO nanoparticles by sol–gel process. *Journal of Materials Science: Materials in Electronics*, 26, 8147-8159.
- Boukhachem, A., Boughalmi, R., Karyaoui, M., Mhamdi, A, Chtourou, R., Boubaker, K., Amlouk, M. (2014). Structural, Morphological and Optical Properties of Nanostructure Nickel Oxide Thin Films on Quartz Substrates Grown by Plasma Oxidation. *Mater. Sci. Eng. B*, 188, 72-77
- Bykkam, S., Ahmadipour, M., Narisngam, S., Kalagadda, V.R., Chidurala, S.C. (2015). Extensive Studies On X-Ray Diffraction of Green Synthesized Silver Nanoparticles. *Adv. Nanopart*., 4, 1–10.
- Chan, M.I., Hsu, Y.T., Hong, C.F. (2002). A Carbon Nanotube Based Resettable Sensor For Measuring Free Chlorine In Drinking Water. *Applied Physics Letters*, 81, 1899.
- Cook, J. G., & Koffyberg, F. P. (1984). Solar Thermal Absorbers Employing Oxides of Ni And Co. *Solar Energy Materials*, *10*(1), 55.
- Cullity, B. (1967). *Elements of X-ray Diffraction*, A.W.R.C. Inc., Massachusetts.
- Farhat, S., Rekaby, M., & Awad, R. (2019). Vickers microhardness and indentation creep studies for erbium-doped ZnO nanoparticles. *SN Applied Sciences*, *1*(6), 546.

- Gaber, A., Abdel-Rahim, M. A., Abdel-Latief, A. Y. and Abdel-Salam, M. N. (2014). Influence of Calcination Temperature on the Structure and Porosity of Nanocrystalline SnO2 Synthesized by a Conventional Precipitation method, *Int. J. Electrochem. Sci*., 9, 81–95.
- Gong, J., Wu, J., & Guan, Z. (1999). Examination of the Indentation Size Effect in Low-Load Vickers Hardness Testing Of Ceramics. *Journal of the European Ceramic Society*, *19*(15), 2625-2631.
- He, J., Lindström, H., Hagfeldt, A., & Lindquist, S. E. (1999). Dye-Sensitized Nanostructured P-Type Nickel Oxide Film as a Photocathode for a Solar Cell. *The Journal of Physical Chemistry B*, *103*(42), 8940.
- Hotovy, I., Rehacek, V., Siciliano, P.,Capone, S., Spiess, L. (2002). Hotovy, I., Rehacek, V., Siciliano, P.,Capone, S., Spiess, L. (2002). Thin Solid Films, 418, 92. *Thin Solid Films*, 418, 92.
- Kazah. Iman, Awad, R. (2017). The Investigation of the Mechanical Properties of Mn Doped $Basno_3$ Nanoparticles. *Journal of Physics: Conference Series*, 869, 012029.
- Kumar, D., Idapalapati,S., Wang, W., Narasimalu,S. (2019). Effect of Surface Mechanical Treatments on the Microstructure-Property-Performance of Engineering Alloys. *Materials* (Basel), 12, 2503.
- Liu, K. C., & Anderson, M. A. (1996). Porous Nickel Oxide/Nickel Films for Electrochemical Capacitors. *Journal of the Electrochemical Society*, *143*(1), 124.
- Singh, P., Kaushal, A., & Kaur, D. (2009). Mn-Doped Zno Nanocrystalline Thin Films Prepared By Ultrasonic Spray Pyrolysis. *Journal of Alloys and Compounds*, *471*(1-2), 11-15.
- Rajkovic, V., Bozic, D., Devecerski, A., & Jovanovic, M. T. (2012). Characteristic Of Copper Matrix Simultaneously Reinforced With Nano-And Micro-Sized Al2O3 Particles. *Materials characterization*, *67*, 129-137.
- Senthilkumar, V., Vickraman, P., Jayachandran, M., & Sanjeeviraja, C. (2010). Structural and Electrical Studies of Nano Structured Sn 1− X Sb X O 2 (X= 0.0, 1, 2.5, 4.5 and 7 at %) Prepared By Co-Precipitation Method. *Journal of Materials Science: Materials in Electronics*, *21*(4), 343-348.
- Shahzad, F., Ettinger, K., Letofsky-Papst, I., Weber, J., Knoll, P. (2015). Preparation and Characterization of Nio Nanoparticles. *Journal of Nano Research*, 31, 93-102.
- Srour, A., Malaeb, W., Rekaby, M., & Awad, R. (2017). Mechanical properties of the (BaSnO3) x/Cu0. 5Tl0. 5Ba2Ca2Cu3O10− δ superconductor phase. *Physica Scripta*, *92*(10), 104002.
- Tosun, M., Ataoglu, S., Arda, L., Ozturk, O., Asikuzun, E., Akcan, D., Cakiroglu, O (2014). Structural and Mechanical Properties of Znmgo Nanoparticles. *Materials Science & Engineering A*, 590, 416-422.
- Wang, S. H., Jian, S. R., Chen, G. J., Cheng, H. Z., & Juang, J. Y. (2019). Annealing-driven microstructural evolution and its effects on the surface and nanomechanical properties of Cu-doped NiO thin films. *Coatings*, *9*(2), 107.
- Yoshimura, K., Miki, T., & Tanemura, S. (1995). Nickel oxide electrochromic thin films prepared by reactive DC magnetron sputtering. *Japanese journal of applied physics*, *34*(5R), 2440.